Analysis of acoustic emission data to estimate true fracture energy of plain concrete

Fracture process in concrete has been the core subject of research in fracture mechanics of concrete. Several models have been developed to explain the fracture process. Upshot of the research studies is the identification of fracture process zone (FPZ) that is formed ahead of the crack tip. Viewing the formation of FPZ has been made possible by new techniques, viz. X-ray, dye penetration and acoustic emission (AE). Also, the extent of heterogeneity of the material has a bearing on the fracture characteristics. AE technique has been applied to study the fracture process in mortar, plain concrete and reinforced concrete to understand the AE characteristics of fracture process[1]. With increased sophistication in capturing and analysis of AE waves, AE technique is becoming a potential tool to comprehend the fracture process in concrete. The FPZ in front of a crack tip in concrete is the consequence of the formation of micro cracks, a few of which later link up to form a macro crack. The formation and growth of cracks are associated with the release of elastic strain energy in the form of AE waves[2,3]. The captured AE data depict the damage process in concrete. The size of the FPZ thus formed could be estimated using the density of event locations from the AE catalogue[4]. The AE technique has also been used in the study of damage and diagnosis of masonry and concrete structures[5–9].

The fracture energy obtained using the fracture method[10] is size-dependent and thus cannot be construed as a material constant. Size effect model[11,12], boundary effect model (BEM)[13–15], multi-scale model with fractals[16] and several other models have been developed to estimate the size-independent fracture energy. A recent addition is the fracture energy release rate method[17]. A hybrid method[4] combining BEM and the data from AE technique to estimate the size-independent fracture energy in concrete is yet another attempt to estimate the true fracture energy of concrete. A recent improved procedure of the hybrid method on fracture of concrete to estimate size-independent fracture energy using AE technique is the tri-linear model[18].

In the present study the density of AE events across the uncracked ligament length is studied to estimate the length of FPZ. The work of fracture, calculated using the load–deflection curve, is assumed to be used up for the formation of FPZ, the length of which is estimated using the AE data. The cross-sectional area of the specimen at the notch with one of the dimensions being the FPZ length and the other being the width of the specimen is assumed as the true fracture area. In this study an attempt has been made to estimate fracture energy using the fracture area from AE data and the work of fracture.

The beam tested had a width of 95 mm, depth of 190 mm and span of 564 mm; notch depth was 49 mm. The concrete used to cast the beam had a compressive strength of 45 MPa. The AE equipment used was from Physical Acoustic Corporation, Princeton, New Jersey, USA. The AE instrument was an eight-channel with AEwin for SAMOS (sensor-based acoustic multi-channel operating system) E2.0 system PAC Manual (2005). The AE instrument has sensors to receive the AE signals, pre-

amplifiers and data acquisition system to acquire and analyse the data. The AE sensor is 19 mm in diameter and 22 mm in height with a resonant frequency of 60 kHz. It was used for AE acquisition and arranged on one face of the specimen as shown in Figure 1. The locations of events have the origin of reference at the bottom left corner of the specimen. The surface of the specimen where the positions of the sensors are marked was initially cleaned with acetone solution to remove dust and to ensure better bonding between sensor and specimen. The AE sensors were fixed to the specimen surface using high vacuum silicone grease or gel. The threshold value was kept at 45 dB to minimize the effect of noise. The sensors were initially tested for their sensitivity by pencil lead-breaking. Further automatic sensor testing (AST) available in the AE software was employed to check the fixity of the sensors to the concrete surface and to ensure that there is no gap between the sensor and the surface.

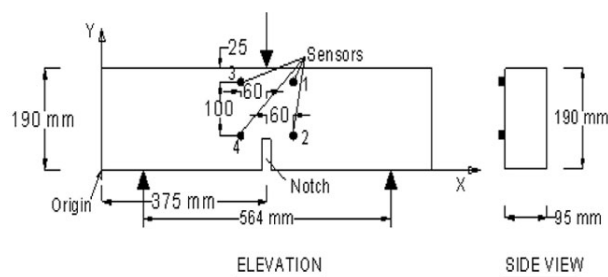From the AE data obtained, the number of events recorded until failure was 691. From each event, the maximum

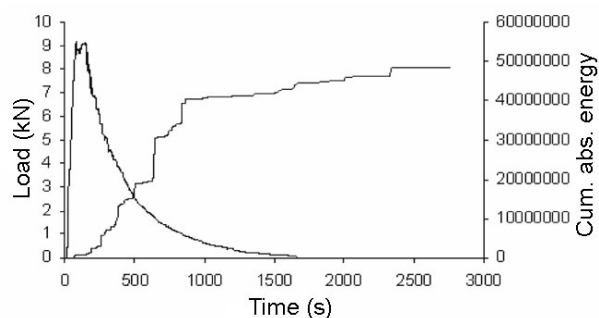**Figure 1.** Profile of the beam showing the position of sensors.

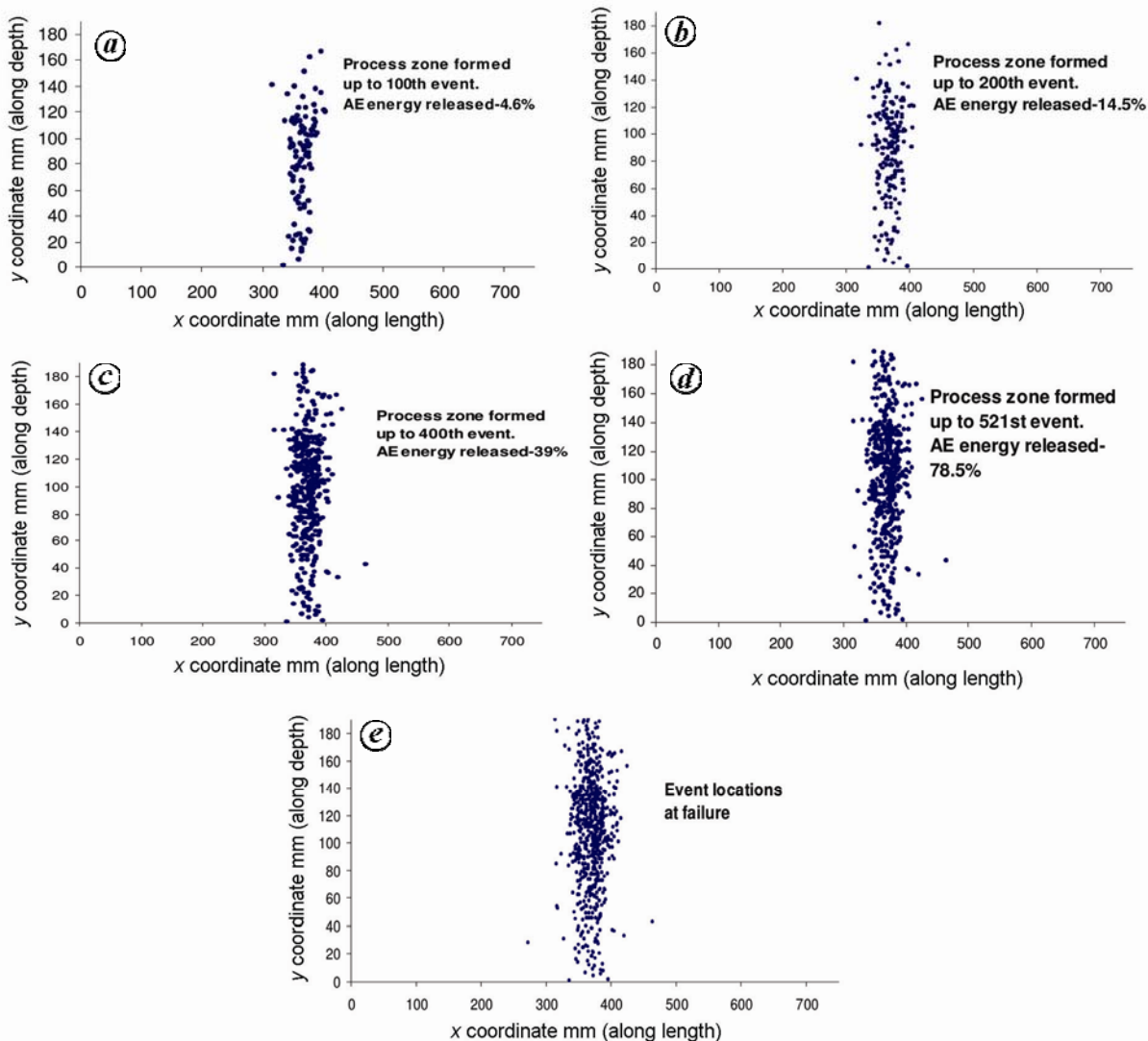**Figure 2.** Load-time–cumulative absolute acoustic emission (AE) energy plot.

Figure 3. Process zone size corresponding to event no. 100 (*a*), event no. 200 (*b*), event no. 400 (*c*), event no. 521 (*d*) and (*e*) event locations at failure.

absolute energy amongst the sensor readings was chosen for the analysis, since this energy is nearest to the actual absolute AE energy released during that event. All the AE parameters such as amplitude, energy, counts, duration, absolute energy, event location coordinates and transit time corresponding to each sensor were separated for ease of accurate analysis.

Figure 2 shows a combined plot of load-time and cumulative absolute energy-time. It evident that the rate of increase of absolute energy is higher initially. This could be due to the formation of micro cracks at closer intervals of time. The absolute energy released from each micro crack formation in short intervals of time accrues and hence increases the rate or, in other words, the slope of the

plot. There are some local steep risers in the plot indicating high energy release rate and the formation of macro cracks. The flatter portions of the plot correspond to the macro crack propagation during which less AE energy is released. Also, as the number of events increases, there is corresponding increase in the number of micro cracks resulting in reduction of stiffness and load-carrying capacity. This is clearly seen from the drop in load level with an increase in time. This analysis strengthens the argument that the time duration from the beginning to the end of the sloped portion of the cumulative absolute energy–time curve represents the time of formation of the FPZ. The number of events that occurred during this time is found to be 521 as against total events of 691, which is

nearly 75% that accounts for the formation of FPZ.

The cumulative energy versus time plot has certain interesting features. It looks similar to elastic–perfectly plastic, stress–strain relationship. Although concrete is not plastic, it shows softening. The events that take place inside seem to reach a plateau similar to the plastic behaviour. The cumulative absolute energies keep increasing till the peak and also beyond the peak in the softening portion of the load–displacement–time plot. When sufficient micro cracks have formed to coalesce to form macro cracks, there is no further increase in the cumulative absolute energy and it reaches a plateau.

The evolution of the FPZ corresponding to different events is shown in Figure 3.

Table 1. Percentage of absolute acoustic emission (AE) energy recorded along the ligament length of the beam

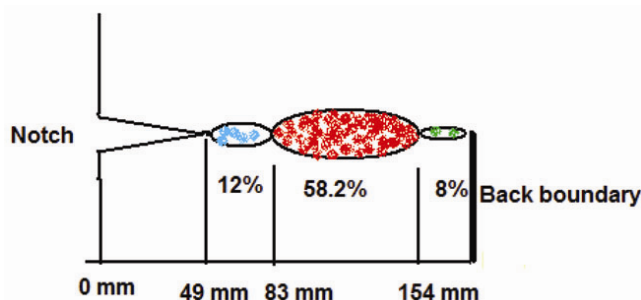| Band width bounded between x coordinates measured along the span of the beam (mm)	Percentage of absolute AE energy recorded up to different y values measured along the depth (ligament length) from the bottom			
	Up to 83 mm	83–118 mm	118–154 mm	154–190 mm
370–380	3.3	15.7	2.5	0.5
365–385	10.2	19.2	19.1	1
360–390	10.4	20	21.2	7.2
355–395	11.8	21.9	21.4	7.3
350–400	12	23.1	21.6	7.7
345–405	12	36	22	8
340–410	12	36	22	8
335–415	12.1	36	22.2	8.2

Figure 4. Schematic diagram showing the regions with percentage of AE energy dissipated along the ligament.
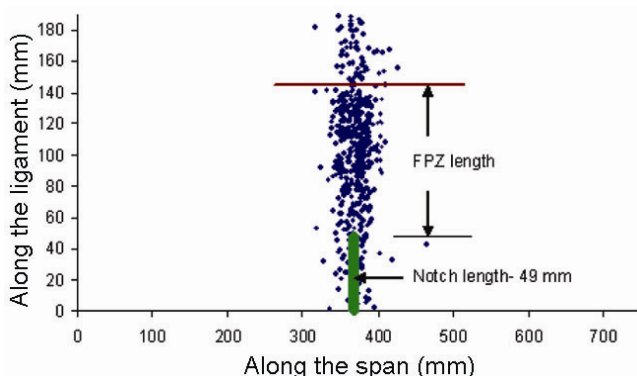

Figure 5. Plot showing the high density of AE events along the ligament length of the beam.

The first event recorded corresponds to about 80% of the peak load of 9.5 kN and this occurred below the notch tip. The AE data acquired until the FPZ formation was analysed and the results are shown in Table 1.

After analysing the AE record, it has been possible to know the quantum of absolute AE energies released in narrow bands on either side of the notch as given in Table 1. A careful observation of the percentage of absolute AE energy recorded along the uncracked ligament length (Table 1) indicates that near the crack tip (up to 83 mm) and near the back boundary (between 118 and 190 mm), the AE energy is about 12% and 8% respectively, while in the interior region it is about 58.2%. This implies that the density of events in the interior region is more than near the back boundary (Figure 4). This observation reaffirms the assumption made earlier[8] that the process zone around a propagating crack is made of two regions, an inner softening region and an outer region with microcracks. Using the AE technique it has been possible to visualize the FPZ formation.

The length of uncracked ligament length over which the density of events is more could be considered as the length of FPZ. From Table 1, it can be seen that up to 154 mm of ligament length from the base of the beam, the density of AE events is significantly higher but declines towards back boundary, where the density is about 8%. With identification of length of ligament in which the density of AE events is higher, it is possible to roughly estimate the length of FPZ (Figure 5) by subtracting the notch length. The zones mentioned in Table 1 like up to 83 mm, 83–118 mm, etc. are arbitrarily chosen for calculation of the number of events. In the present case the density is relatively high in the zone 118–154 mm. However, except for a few events beyond 144 mm up to 154 mm most are within 144 mm. Therefore, the limit 49–144 mm is considered as FPZ, which is approximately shown in Figure 5.

The RILEM fracture energy, based on work of fracture, is calculated by considering the entire uncracked ligament length along with the width of the beam. Though the entire uncracked ligament length does not account for FPZ size, it is considered in the calculation of fracture area, due to which the fracture energy calculated is not the true fracture energy. In the present study, after having estimated the length of FPZ in the sample beam through AE technique, an attempt has been made to obtain the fracture energy using the estimated FPZ length. The width of the beam is 95 mm. The entire width of the beam at the notch is assumed to be part of FPZ and the fracture area calculated is 9095 mm^2. The work of fracture obtained for the beam from the experiment is 1971 N-mm. The fracture energy calculated from the above data is 216.7 N/m. The beam

whose AE data are analysed and presented in the present work is a part of the set of beams considered in the study using tri-linear model[18]. The size-independent fracture energy calculated using the tri-linear model[18] was 219.6 N/m, which is fairly close to the value estimated in the present study. This confirms that the above method, although approximate, gives fairly reasonable values of size-independent fracture energy.

Thus the present study reaffirms not only the versatility of the AE technique to visualize FPZ formation in real time, but also its usefulness in estimating the size of FPZ and consequently the size-independent fracture energy. The FPZ estimated using the AE technique, having higher density of events in the interior and lesser density surrounding it, substantiates the assumption made in the BEM regarding FPZ. The FPZ length estimated using AE technique is useful in calculating the true fracture energy. The true fracture energy calculated from the present method, which could be viewed as an approximate method, is 216.7 N/m. This is in good agreement with the size-independent fracture energy of 219.6 N/m estimated using the tri-linear model[18].

1. Wu, K., Chen, B. and Yao, W., *Cem. Concr. Res.*, 2000, **30**, 1495–1500.
2. Mindess, S., *Int. J. Cem. Comp. Light Wt. Conc.*, 1982, **4**, 173–180.
3. Ohtsu, M., *Mag. Concr. Res.*, 1996, **48**, 321–330.
4. Muralidhara, S., Raghu Prasad, B. K., Eskandari, H. and Karihaloo, B. L., *Constr. Build. Mater.*, 2010, **24**, 479–486.
5. Carpinteri, A. and Bocca, P., *Damage and Diagnosis of Materials and Structures*, Pitagora, Bologna, 1991.
6. Carpinteri, A. and Lacidogna, G., In Proceedings of the 9th International Congress on Sound and Vibration (ICSV9), Orlando, FL, USA, 2002.
7. Carpinteri, A. and Lacidogna, G., *J. Facta Univ.*, 2003, **3**, 755–764.
8. Carpinteri, A., Lacidogna, G. and Pugno, N., In Proceedings of the 5th International Conference on Fracture Mechanics of Concrete and Structures (FramCos-5) (eds Li, V. C. *et al.*), Vail, CO, USA, 2004, pp. 31–40.
9. Carpinteri, A., Lacidogna, G. and Pugno, N., *Acoust. Tech.*, 2004, **38**, 2004, 31–37.
10. RILEM FMC-50. *Mater Struct.*, 1985, **18**, 287–290.
11. Bažant, Z. P. and Pfeiffer, P. A., *ACI Mater. J.*, 1987, **84**, 463–480.
12. Bažant, Z. P. and Kazemi, M. T., *Int. J. Fract.*, 1990, **44**, 111–131.
13. Duan, K., Hu, X. and Wittmann, F. H., *Eng. Fract. Mech.*, 2003, **70**, 2257–2268.
14. Duan, K., Hu, X. Z. and Wittmann, F. H., *Eng. Fract. Mech.*, 2007, **74**, 87–96.
15. Karihaloo, B. L. and Xiao, Q. Z., *Sādhanā*, 2002, **27**, 449–459.
16. Carpinteri, A., Chiaia, B. and Cornetti, P., *Eng. Fract. Mech.*, 2003, **70**, 2321–2349.
17. Muralidhara, S., Raghu Prasad, B. K. and Singh, R. K., *Eng. Fract. Mech.*, 2013, **98**, 284–295.
18. Muralidhara, S., Raghu Prasad, B. K., Karihaloo, B. L. and Singh, R. K., *Constr. Build. Mater.*, 2011, **25**, 3051–3058.

S. MURALIDHARA[1,*]
B. K. RAGHU PRASAD[2]
R. K. SINGH[3]

[1]Department of Civil Engineering,
BMS College of Engineering,
Bangalore 560 019, India
[2]Indian Institute of Science,
Bangalore 560 012, India
[3]Reactor Safety Division,
Bhabha Atomic Research Centre,
Mumbai 400 085, India
*For correspondence.
e-mail: smuralidharabms@gmail.com

Colonization and antagonistic activity of entomopathogenic *Aspergillus* sp. against tea termite (*Microcerotermes beesoni* Snyder)

Tea (*Camellia sinensis* L.) is widely planted in the tropical and subtropical zones, including India, China, Vietnam, Japan and Sri Lanka. India produces 35% of the world's tea, and its 400,000 ha land in the northeast region is under tea cultivation[1]. However, despite the availability of improved technology, nutrition and fertility management[2], biotic stresses like insect pests and diseases limit the productivity of tea[3,4], resulting in 11–55% annual loss in yield[5]. Termites include more than 2600 species around the world[6], but only few (70–80 species) are considered of economic importance. In India, there are eight species of termites that cause damage to tea plants, out of which *Microcerotermes beesoni* Snyder, *M. obesi* Holmgern and *Odontotermes*

feae have been identified and confirmed by the Zoological Survey of India, Kolkata[7] from the Barak valley, Assam. There has been heavy usage of organo-synthetic pesticides since 1950s against termites, leading to rapid conversion of innocuous species into pests, development of resistance, and undesirable pesticide residues in tea. As a result, pesticide residues have become a major problem for the tea industry[5]. This raises an urgent need for the use of biocontrol measures for termite control. In the Barak valley, infestation of termite is the predominant cause that limits tea production. Therefore, the present work was undertaken with an objective to isolate the entomopathogenic microorganisms and study their biocontrol/colonization

ability against tea termites infesting live wood tea plants of the tea gardens in Barak valley.

A dark chamber was designed to provide a suitable environment for the termites in laboratory condition. It was prepared by wrapping black paper inside a box on all sides. Normal or tap water of about 50–100 ml was sprayed over the nest. The colonies were maintained at $27 \pm 2°C$ and 70–80% relative humidity by keeping in a cool, dark area. A piece of nest collected from the tea garden was gently crushed and termites were transferred and trapped with the help of smooth fibre brush. The tea termites were identified as *M. beesoni* Snyder on the basis of morphological characteristics, mainly mandibular region and antennal part.